Tellus SERIES A DYNAMIC METEOROLOGY AND OCEANOGRAPHY
PUBLISHED BY THE INTERNATIONAL METEOROLOGICAL INSTITUTE IN STOCKHOLM

Tellus (2009), 61A, 381–393

TELLUS

Running GCM physics and dynamics on different grids: algorithm and tests

By ANDREA MOLOD[1,2]*, [1]*Goddard Earth Sciences and Technology Center, University of Maryland Baltimore County, Baltimore, MD, USA;* [2]*Global Modeling and Assimilation Office, NASA Goddard Space Flight Center, Greenbelt, MD, USA*

(Manuscript received 15 November 2007; in final form 13 January 2009)

ABSTRACT

An 'alternate grid' (GridAlt) technique is presented, which allows the different components of a general circulation model's governing equations to be computed on distinct grids chosen for that component or process. In the implementation presented here, the tendencies of state variables from the physical parametrizations are computed on a vertical grid with very fine resolution near the surface, whereas the remaining terms in the equations of motion are computed using an Eta coordinate with coarser vertical resolution.

Results from a suite of aquaplanet experiments show that much of the benefit of increased vertical resolution in the whole model can be realized by enhancing the vertical resolution of the 'physics grid' using GridAlt. The benefit is realized in the fields which are computed directly in the physical parametrizations, and in the vertical structure of the relative humidity and mass streamfunction. Results from a suite of realistically configured simulations demonstrated an impact of GridAlt that was similar to its impact in the simplified simulations, as well as an improved response to El Niño Southern Oscillation forcing. It is concluded that the present implementation of GridAlt offers a practical way to allow GCMs to better capture the near-surface structure of the atmosphere.

1. Introduction

The vast majority of atmospheric general circulation models (GCMs) currently in use for climate study and numerical weather prediction require the computation of all the terms in the equations of motion on a single grid. This includes the terms that represent the resolved processes as well as the model closure or 'parametrization forcing' (or 'physics' forcing) terms, which arise from estimates of the net effect of unresolved physical processes on the resolved scales. The scales of atmospheric variations to which these unresolved processes respond occur on scales that are much smaller than the resolved scale, and the ability to compute the closure terms on the grid most appropriate to the parametrization of these processes may result in improvements in GCM simulations.

The use of a separate horizontal discretization for the physics forcing was developed by Vintzileos and Sadourney (1997) to allow the physics grid to follow the underlying surface, in particular, near coastlines or sea ice boundaries. The recognition of the need for a separate vertical discretization for the physics underlies the scheme developed by Lock (2000), for example, in which the sharp gradients across the boundary layer top are modelled by dividing the grid box vertically into two separate layers. In addition, the need for much finer resolution to capture the effects of cumulus convection on the GCM grid scale motivates the cumulus superparametrization schemes of Grabowski (2001) and others. The implementation of the new technique presented in the present study addresses the need for a separate and finer vertical grid for the entire suite of parametrizations that make up the GCM physics.

The desirability of fine vertical resolution near the surface can be argued on physical grounds and has been demonstrated in numerical experiments. The vertical length scales near the ground are small and can vary on short timescales. In addition, the vertical length scale of the turbulence depends on the distance above the surface. This results in the presence of a fine-scale vertical structure in the atmosphere, and the vertical grid must be adequate to resolve the smaller length scales to capture, for instance, the diurnal variation of the planetary boundary layer and the associated diurnal variations in the vertical structure of temperature and momentum. Studies with both regional and global atmospheric models have demonstrated improvements when the vertical resolution near the surface is increased. The improvements were often related to the behavior of the turbulent and convective parametrizations at the higher resolution. Bushell and Martin (1999), for example, reported a better simulation of

*Correspondence
e-mail: Andrea.Molod@nasa.gov
DOI: 10.1111/j.1600-0870.2009.00394.x

the boundary layer structure and of boundary layer clouds when the number of levels inside the boundary layer was increased from 3 to 9. Inness et al. (2001) found that the propagation speed of the Madden-Julian Oscillation (MJO) was improved in a simulation with increased vertical resolution and postulated that the higher correlation between warm sea surface temperatures and precipitation in the higher resolution simulation underlays the improved MJO.

The potential advantage of a separate 'physics grid' for the vertical discretization is brought to focus within the context of a model that employs a vertical coordinate that does not follow the terrain. For example, the most recent version of the NCEP Eta-coordinate model is discretized using 60 vertical levels, and the resolution near the surface at sea level is close to 20 m. The near-surface resolution when the surface is at 850 HPa, however, is degraded to near 170 m (Rogers et al., 2001). The consequences of insufficient vertical resolution near the surface over terrain in an older version of the NCEP Eta model have been summarized by Staudenmaier and Mittelstadt (1997), who concluded that the relatively coarse vertical resolution near the surface over the western United States resulted in simulated surface winds that are too weak and surface temperatures that are too cold. A separate 'physics grid' in a GCM with a pressure coordinate could allow at least some of the bias due to the coarse resolution of the 'dynamics grid' to be alleviated without incurring prohibitive computational costs.

A technique to allow the 'physics' forcing terms, or closure terms, to be computed on their own vertical grid has been developed for the MITgcm and is presented here, called the 'GridAlt' technique. Two suites of simulations were performed to evaluate the ability of a GCM with GridAlt to capture the near-surface atmospheric structure compared with high resolution GCM experiments as well as observations. The GridAlt technique is presented in Section 2, along with some implementation details. A brief description of the GCM is presented in Section 3. Results from the suites of simplified and realistic GCM experiments, which evaluate the impact of the technique, are presented in Sections 4 and 5. Finally, Section 6 includes a summary and a discussion of other potential uses of the GridAlt technique.

2. The GridAlt algorithm

Parametrizations of atmospheric subgrid scale processes are all essentially concerned with one model grid cell at a time. The vertical grid on which the tendencies provided by these parametrizations are computed (the 'physics grid') can be entirely independent of the grid on which the equations of motion are integrated (the 'dynamics grid'). The GridAlt technique, presented here, allows the tendencies due to the physical parametrizations to be computed using a vertical discretization with very fine resolution near the surface. GridAlt also allows the resulting finer scale vertical structure of the atmosphere to be 'remembered' between model time steps. GridAlt allows this by retaining the state variables on both the high resolution 'physics grid' and the coarser resolution 'dynamics grid' and ensures that the two estimates of the state 'agree' on the 'dynamics grid'. This handling of the 'physics' terms allows the parametrizations of cumulus convection and turbulence, in particular, to make use of the enhanced gradients of the mean flow, which can be resolved by the finer resolution grid near the surface.

The 'physics grid' adjusts to the local terrain and contains additional levels near the surface in each vertical column, thus guaranteeing high resolution near the ground. The vertical discretization in the physics for the column above each gridpoint is therefore distinct. For convenience, the levels of the physics grid are constrained to fit exactly into the existing dynamics grid, simplifying the interpolations back and forth between the two vertical grids. The physics and dynamics grids are illustrated schematically in Fig. 1, where the grey regions represent the mountains, the thick black lines represent the 'dynamics grid' levels and the thinner black lines represent the additional 'physics levels' added near the surface for each grid box. The levels refer to the level centre, and the level spans from its bottom edge (defined as half the distance to the nearest level centre) to its top edge.

In addition to computing the physical forcing terms of the momentum, thermodynamic and humidity equations on the physics (higher resolution) grid, GridAlt includes an integration of a second set of evolution equations for the atmospheric state variables on the physics grid. The equation for the evolution of T (representing temperature, for example) on the dynamics grid can be expressed as

$$\Delta T\big|_{\text{dyn}}^{\text{total}} = \Delta T\big|_{\text{dyn}}^{\text{dynamical forc}} + \Delta T\big|_{\text{dyn}}^{\text{physical forc}}, \quad (1)$$

where dyn refers to the dynamics grid and the physical forcing terms on the dynamics grid have been interpolated from the physics grid. An additional equation governing the evolution of

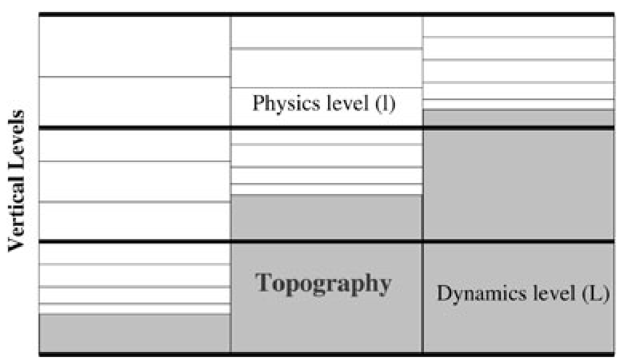

Fig. 1. Schematic of the vertical discretization for the 'Physics grid' (thin lines) and the 'Dynamics grid' (thick lines). The topography is represented by the grey blocks.

T, integrated on the physics grid is written

$$\Delta T|_{\mathrm{phys}}^{\mathrm{total}} = \Delta T|_{\mathrm{phys}}^{\mathrm{dynamical\ forc}} + \Delta T|_{\mathrm{phys}}^{\mathrm{physical\ forc}} + \gamma(T|_{\mathrm{dyn}} - T|_{\mathrm{phys}}) \qquad (2)$$

where phys refers to the physics grid, and the dynamical forcing terms have been interpolated from the dynamics grid. The last term on the right-hand side is a relaxation term, which ensures that the state variables at the new time level on the physics grid 'track' the state variables on the dynamics grid on some timescale, governed by γ. In the present implementation, $\gamma = 1$, requiring an immediate agreement between the two 'states' at each time step. This term was generally found during integrations to be two orders of magnitude smaller than the other terms and so does not contribute significantly to the simulation, but is, nonetheless, needed. Integrating separate evolution equations on the different grids in use during the GCM simulation is also performed as part of the cumulus superparametrization scheme of Grabowski (2001) and also serves as a 'memory' of the fine scale structure from one GCM time step to the next.

If we write T_{phys} as the temperature on the high resolution physics grid, and T_{dyn} as the temperature on the coarse vertical resolution dynamics grid, then the algorithm can be expressed by the following steps:

(1) Compute the tendency due to physical processes.

(2) Advance the physics state:

$$T^{n+1^{**}}{}_{\mathrm{phys}}(l) = T^{n}{}_{\mathrm{phys}}(l) + \delta T_{\mathrm{phys}}, \qquad (3)$$

where l represents any level on the physics grid (See Fig. 1).

(3) Interpolate the physics tendency terms to the dynamics grid (See Fig. 1), and advance the dynamics state by physics and dynamics tendencies

$$T^{n+1}{}_{\mathrm{dyn}}(L) = T^{n}{}_{\mathrm{dyn}}(L) + \delta T_{\mathrm{dyn}}(L) + [\delta T_{\mathrm{phys}}(l)](L), \qquad (4)$$

where L represents any level on the dynamics grid and [ ] is the interpolation from the physics to the dynamics grid.

(4) Interpolate the dynamics tendency terms to the physics grid, and update the physics state with those tendencies:

$$T^{n+1^{*}}{}_{\mathrm{phys}}(l) = T^{n+1^{**}}{}_{\mathrm{phys}}(l) + \{\delta T_{\mathrm{dyn}}(L)\}(l). \qquad (5)$$

Here { } is the interpolation from the dynamics to the physics grid.

(5) Apply a correction term to the physics state to account for any deviation from the dynamics state on the dynamics grid:

$$T^{n+1}{}_{\mathrm{phys}}(l) = T^{n+1^{*}}{}_{\mathrm{phys}}(l) + \gamma\{T^{n+1}{}_{\mathrm{dyn}}(L) - [T^{n+1^{*}}{}_{\mathrm{phys}}(l)](L)\}(l). \qquad (6)$$

The GridAlt algorithm does not directly impact the computation of the dynamical tendency terms nor their application on the dynamics grid. It affects only the computation of the physical tendency terms in the equations of motion. The interpolations from coarse to fine and back, therefore, as well as the correction term, may be regarded as modifications to the physical parametrizations in that they alter the physical tendency terms added to the equations of motion on the dynamics grid. A desirable feature of the interpolation scheme is that the correction term itself does not create a non-zero physical tendency when the parametrizations do not produce one on the physics grid. To accomplish this and minimize the contribution of the interpolation between grids to the correction terms, all the interpolations between the vertical grids were constructed so that a dynamics-to-physics interpolation can be exactly reversed with a physics-to-dynamics interpolation. The simple scheme employed to achieve this is as follows.

Dynamics to physics: For all physics levels l in dynamics level L, assign the dynamics grid value to each physics grid level

$$\delta T_{\mathrm{phys}}(l) = \{\delta T_{\mathrm{dyn}}(L)\} = \delta T_{\mathrm{dyn}}(L)\mathrm{weight}(l) \qquad (7)$$

where the weights are set to 1 for temperature and moisture, and to

$$\mathrm{weight}(l) = \frac{\sqrt{u(l)^2 + v(l)^2}\,\delta p(l)}{\frac{1}{\delta p(L)}\sum_l \sqrt{u(l)^2 + v(l)^2}\,\delta p(l)} \qquad (8)$$

for the momentum components. The weights chosen for the interpolation of temperature and moisture have the potential to result in the creation of spurious gradients between physics levels in adjacent dynamics levels under conditions of large gradients in the dynamic tendencies of those fields, but there is no evidence in the results of the creation of large gradients. The weighting factor for momentum is designed to preserve the physics grid profile of momentum when the dynamical forcing is interpolated to the physics grid and added to the physics state momentum variables.

Physics to dynamics: For each dynamics level L and all physics levels l contained therein, compute the pressure-weighted average of the physics grid values:

$$\delta T_{\mathrm{dyn}}(L) = [\delta T_{\mathrm{phys}}(l)] = \frac{1.}{\delta p(L)} \sum_l \delta T_{\mathrm{phys}}(l)\delta p(l). \qquad (9)$$

The bottom 200 hPa segment of the profiles which result from this interpolation scheme is illustrated in Fig. 2. The vertical dashed lines are the edges between dynamics grid levels, and the interpolation example shown here is from the 20 dynamics level (and 27 physics level) model configuration depicted in the middle panel of Fig. 3. The sequence shown in the figure is an interpolation from the physics grid to the dynamics grid, from the dynamics grid to the physics grid and back again from the physics grid to the dynamics grid. The solid lines with stars represent the original profiles on the physics grid. The dotted lines with open circles (and the dot-dashed lines with x's) show the profiles interpolated to the dynamics grid, where the dynamics grid values are the average of the physics grid values contained in each dynamics level. The dashed lines with plus signs show the profiles interpolated back to the physics grid. The dashed line

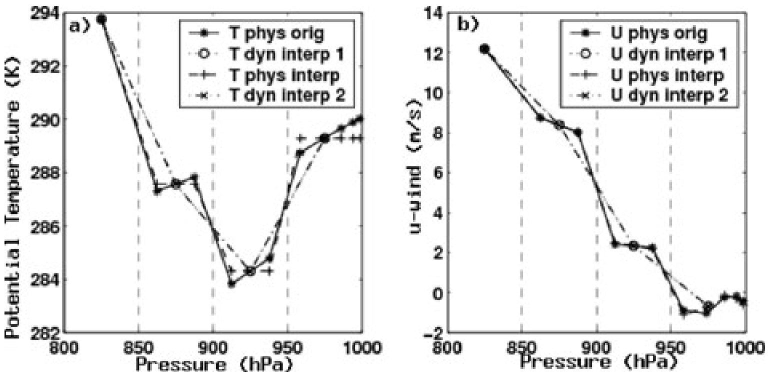

Fig. 2. Example profile showing the results of the interpolation scheme. (a) Profile of potential temperature in K. Lines are as follows: solid star is for the initial profile on the physics grid; dotted circle is for the profile interpolated to the dynamics grid; dashed plus is for the profile re-interpolated back to the physics grid and dot–dash x-symbol is for the profile interpolated back again to the dynamics grid. (b) Same as (a) but for the profile of u-wind in m s^{-1}.

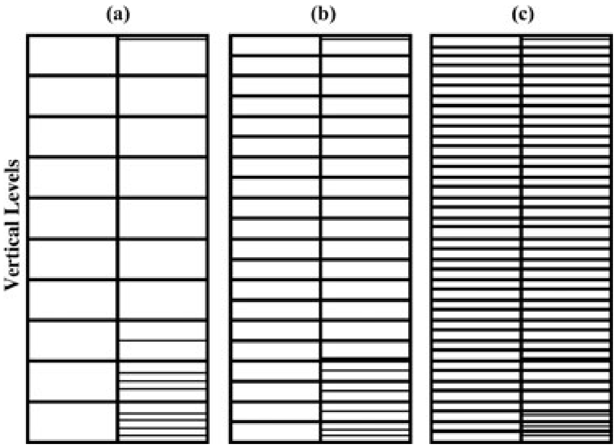

Fig. 3. (a) Distribution of vertical levels for the low-resolution series of experiments, depicting the control, GridAlt and fully resolved aquaplanet experiments. The control is the coarse resolution on the left-hand panel. In the GridAlt simulation, the dynamics is run with the coarse resolution on the left-hand side and the physics with the finer resolution on the right-hand side, and in the fully resolved experiment both dynamics and physics are run using the finer resolution on the right-hand side. (b) and (c) Same as (a) but for the medium and high vertical resolution experiments, respectively.

of Fig. 2a, depicting the scheme used for temperature and humidity, shows the dynamics grid value assigned to each physics grid level contained in that dynamics level, and the dashed line of Fig. 2b, depicting the scheme used for the horizontal components of momentum, shows the physics grid values weighted by the wind speed on the original physics grid. The dotted circle lines are completely covered by the dot–dashed lines, demonstrating that the sequence of interpolation from dynamics grid to physics grid and back again recovers the original profile on the dynamics grid.

3. Description of model and grid

Experiments to evaluate the GridAlt technique were performed with the MIT general circulation model (MITgcm). The MITgcm contains a versatile dynamical core, which can be configured to simulate either atmospheric or oceanic flow (Marshall et al., 2004). The MITgcm in the atmospheric configuration used for the experiments reported here solves the equations on a cubed sphere grid in the horizontal (Adcroft et al., 2004) and on a modified pressure ($p*$) coordinate (Adcroft and Campin, 2004) in the vertical, which makes use of a finite volume 'partial cell' approach for the lower boundary (Adcroft et al., 1997). The atmospheric physical parametrizations in the configuration of MITgcm used for the present experiments is an MITgcm package called Fizhi (Molod et al., 2007), adapted from the GEOS-3 GCM suite of parametrizations. Fizhi includes parametrization schemes for atmospheric convection, large-scale precipitation and cloud cover, long-wave and short-wave radiation, turbulence, gravity wave drag and a land surface model. Multi-year simulations with MITgcm using Fizhi have been performed as part of the participation in the Aquaplanet Experiment (APE; Neale and Hoskins, 2001), and a series of 10-year simulations driven by climatological sea surface temperatures has been performed to evaluate the climate characteristics compared with available observations (Molod et al., 2007). The MITgcm at a horizontal resolution of approximately 2.7° was used to perform two suites of simulations to evaluate the GridAlt technique, a simplified aquaplanet suite and a realistic configuration suite. The experiments that make up both of these suites are listed in Table 1.

4. Aquaplanet suite

4.1. Aquaplanet experiments

The aquaplanet experiments are configured from the control experiment of the suite proposed by Neale and Hoskins (2001) and underly the APE model intercomparison project, designed to examine the behavior of the physical parametrizations of the participating GCMs in a framework that is simpler than a realistic climate simulation. This framework has been shown by Medeiros and Stevens (2007) to exhibit the important climate sensitivity that the more realistic framework exhibits, and the

Table 1. List of control and Gridalt experiments

Aquaplanet	
Low resolution	
Dyn10C	Uniform 100 hPa resolution in Dyn and Phys
GA10/21	Uniform 100 hPa resolution in Dyn, enhanced in Phys
Dyn19	Enhanced resolution near surface in Dyn and Phys
Med resolution	
Dyn20C	Uniform 50 hPa resolution in Dyn and Phys
GA20/29	Uniform 50 hPa resolution in Dyn, enhanced in Phys
Dyn26	Enhanced resolution near surface in Dyn and Phys
High resolution	
Dyn40C	Uniform 25 hPa resolution in Dyn and Phys
GA40/45	Uniform 25 hPa resolution in Dyn, enhanced in Phys
Dyn44	Enhanced resolution near surface in Dyn and Phys
Realistic	
Clim SST	
CtlClim	Uniform 25 hPa resolution in Dyn and Phys
GAClim	Uniform 25 hPa resolution in Dyn, enhanced in Phys
Obs SST	
CtlSST	Uniform 25 hPa resolution in Dyn and Phys
GASST	Uniform 25 hPa resolution in Dyn, enhanced in Phys

reduced dimensionality makes it an attractive framework for isolating the sensitivity to changes in resolution.

An important motivation for running the aquaplanet suite of experiments is related to the standard for evaluation of the GridAlt technique possible with this relatively simpler configuration that specifies zero topographic height everywhere. The 'fully resolved' experiment of each resolution grouping in the aquaplanet suite of Table 1 provides the measure by which the GridAlt experiment is gauged. The use of a modified pressure coordinate in MITgcm makes this experiment, the clear standard for gauging the success of the GridAlt technique, possible only when there is no topographic variation. Successful results of the GridAlt technique are gauged, then, by similarities between the GridAlt experiment and the fully resolved experiment. Similarities between the GridAlt experiment and the uniform resolution experiment represent aspects of the simulations for which the enhanced resolution in the physics has little impact on the solution. The largest impact of the GridAlt experiments is expected in the lower levels of the atmosphere, where the additional resolution exists. Here the expectation is that the impact is manifested in the physical tendencies due to turbulence and moist heating, in the radiative tendencies where the cloud cover is affected and, ultimately, in the meridional wind field and relative humidity (RH).

Although some of the potential advantage of using the GridAlt technique in a pressure coordinate model is lost in a simulation with no surface topography, the use of the full suite of physical parametrizations provides an indication of the behavior of the model and its physical parametrizations with the GridAlt technique employing enhanced resolution for the 'physics' only.

The aquaplanet experiments are performed using an idealized lower boundary with no topography or land and an analytical distribution of sea surface temperatures that is axisymmetric and symmetric about the equator. The solar forcing is the diurnal cycle for the March equinox, resulting in 'perpetual equinox' simulations. Three sets of 3.5-year long (1276 'perpetual equinox' days) aquaplanet experiments were run at various vertical resolutions, as listed in Table 1. Each set includes a uniform resolution experiment, the 'control', where the dynamics and physics tendencies are computed on the same grid (these are the Dyn10c, Dyn20c and Dyn40c experiments of Table 1), a 'GridAlt' experiment in which the dynamics tendencies are computed on a uniform vertical grid and the physics tendencies on a vertical grid enhanced near the surface (these are the GA10/21, GA20/29 and GA40/45 experiments in Table 1) and another experiment, considered the 'fully resolved' experiment, in which both dynamics and physics tendencies are computed on the same vertical grid as the physics in the GA experiments (These are the Dyn19, Dyn26 and Dyn44 experiments in the table). The three sets of experiments were conducted based on 100, 50 and 25 hPa vertical spacing, respectively. The vertical discretization used for each of these experiments is shown in Fig. 3. The thick lines in the figure represent the dynamics levels and the thinner lines represent the additional levels on which the physical parametrizations are evaluated and the 'physics state' is integrated in the GridAlt experiments, and on which both physics and dynamics are computed in the 'fully resolved' experiments.

4.2. Aquaplanet results

A clear impact of the GridAlt technique was found in the series of experiments at low (nominally 100 hPa) and medium (nominally 50 hPa) vertical resolution. These vertical resolutions would be typical of long-term GCM experiments. The immediate influence of the enhanced vertical resolution in the physics and/or in the dynamics is examined by comparing the fields of the tendencies due to the physical processes themselves, such as the convection and turbulence. The extent to which that influence has permeated into the mean flow is examined by comparing the mass streamfunction and RH fields.

Figure 4a–c shows the zonal mean moist heating for the three low-resolution experiments, Dyn10C (Fig. 4a), GA1021 (Fig. 4b), and Dyn19 (Fig. 4c). Figure 4c, which is the fully resolved experiment and the 'truth' for the purposes of these comparisons, shows an elevated heat source due to moist processes and a heat sink at the surface. Figure 4a, the control experiment with uniform 100 hPa resolution, cannot capture the elevated source or the surface sink. Instead, the Dyn10c moist

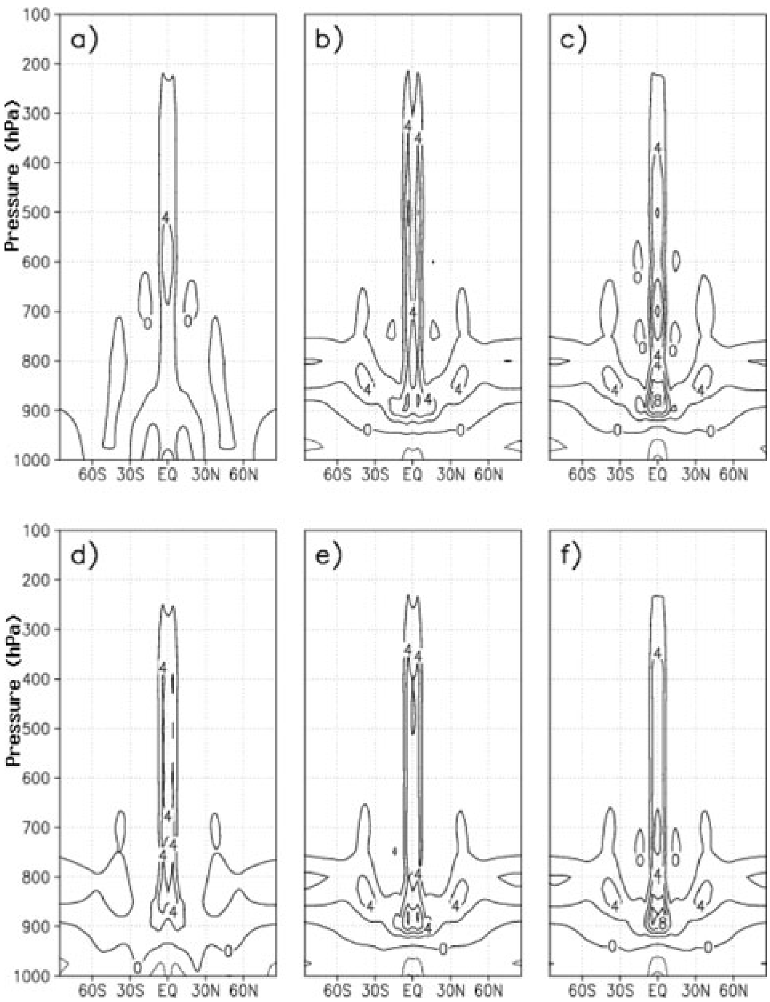

Fig. 4. (a) Zonally averaged moist heating in degree d^{-1} from the Dyn10c experiment. Contour interval is 2° d^{-1}. (b) and (c) Same as (a) but for GA1021 and Dyn19, respectively. (d)–(f) Same as for (a)–(c) but for the Dyn20c, GA2029 and Dyn26 experiments, respectively.

heating field exhibits a maximum at the surface and another aloft near 600 hPa. The GridAlt result, Fig. 4b, shows a clear elevated heating maximum and surface heat sink, although the tropical heating maximum at just above 900 hPa is weaker by up to 2° d^{-1} than in the fully resolved result. Moist heating fields from the medium resolution experiments are shown in Figs. 4d, c and f. The close agreement between the moist heating in the fully resolved experiments, Dyn 19 (Fig. 4c), Dyn26 (Fig. 4f) and Dyn44 (not shown), suggests that the fully resolved solution is indeed a robust 'truth' for these comparisons. Figure 4d shows that the uniform 50 hPa resolution experiment, Dyn20c, captures the surface heat sink, but that the elevated maximum in the tropics is higher in the atmosphere than in the fully resolved result (Fig. 4f), and the maximum in the extratropics is smaller by up to 1.5° d^{-1}. Both the elevation of the tropical elevated maximum and the magnitude of the extratropical maxima are well captured in the result of the GridAlt experiment, Fig. 4e.

The general trend seen in the moist heating is also evident in the cloud field, an indicator of the impact of the moist processes on both the shortwave and longwave radiative heating. Figure 5 shows the cloud fraction from the low- and medium-resolution experiments. For both the low- (top row) and medium-resolution (bottom row) experiments, the pattern shown in the fully resolved experiment (Fig. 5; right-hand panels) is well captured in the GridAlt experiments (Fig. 5; central panel) but not in the control experiment (Fig. 5; left-hand panels). This behavior further affirms the ability of the GridAlt simulations to capture the basic features of the calculations performed in the physical parametrizations of the fully resolved simulation. This behavior is also repeated in the turbulent kinetic energy field, an indicator of the direct results from the turbulence parametrization, and the radiative heating fields (not shown). Many of the figures, which contain results of the 'physics' fields, show a subtle feature at the equator, which is manifested in a local minimum or maximum on the equator. This feature is an artefact of the interpolations to and from the cubed sphere grid used for all the simulations.

The impact of GridAlt on the mean hydrological structure of the various simulations is shown in Fig. 6, the RH field of the low- and medium-resolution experiments. The fully resolved

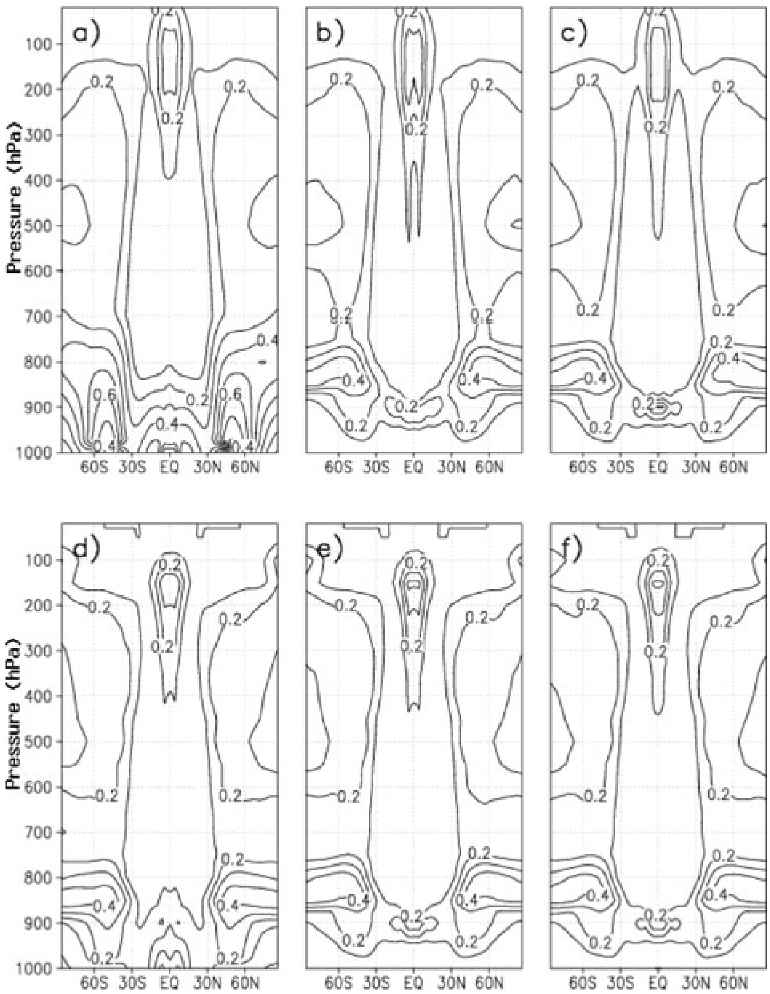

Fig. 5. (a) Zonally averaged cloud fraction from the Dyn10c experiment. Contour interval is 0.1. (b) and (c) Same as (a) but for GA1021 and Dyn19, respectively. (d)–(f) Same as for (a)–(c) but for the Dyn20c, GA2029 and Dyn26 experiments, respectively.

experiments at both resolutions, Figs. 6c and f, show an elevated RH maximum at all latitudes and a region of high RH (greater than 60%) from the surface up to approximately 850 hPa in the tropics and up to approximately 800 hPa at polar latitudes. At 100hPa resolution, the control simulation (Fig. 6a) cannot capture the elevated maximum in the tropics or the vertical extent of the region of high RH near the surface. The GridAlt low-resolution experiment (Fig. 6b) does not capture the elevated maximum in the tropics but does simulate a thicker region of high RH at the surface relative to the control experiment. At the medium resolution, the control experiment (Fig. 6d) still cannot capture the elevated RH maximum in the tropics but does capture a somewhat expanded region of high RH near the surface relative to the low-resolution control. The GridAlt medium resolution experiment, however, seen in Fig. 6e, does capture both the elevated tropical RH maximum and the nearly 200 hPa thick region of RH greater than 80%. The RH field, therefore, indicates an improved simulation near the surface with the use of GridAlt, particularly, in the medium resolution experiments.

The greatest impact on the circulation from changes in the forcing due to the physical parametrizations is expected in the mass streamfunction, shown in Fig. 7 for the low- and medium-resolution experiments. At both low and medium resolutions, the results show the strengthening of the circulation in the fully resolved experiment (Figs. 7c and f) relative to the corresponding control (Figs. 7a and d, respectively). This is shown by the presence of the 20×10^9 kg m^{-2} contour in the fully resolved experiments. The GridAlt experiment at low resolution captures more than half of the difference in magnitude between the control and fully resolved experiments (the maximum in the control is 17 10^9 kg m^{-2}, in GridAlt is 21×10^9 kg m^{-2} and in the fully resolved is 23×10^9 kg m^{-2}) and at medium resolution captures almost all of it. As was the case for the RH field, the mass streamfunction field shows an improved simulation due to the use of GridAlt, and the improvement is greater in the medium resolution experiment than in the low-resolution experiment. This enhanced impact on the mean meridional wind field from the use of GridAlt in the 50 hPa resolution experiment is in contrast to the results of the tendencies from the physical

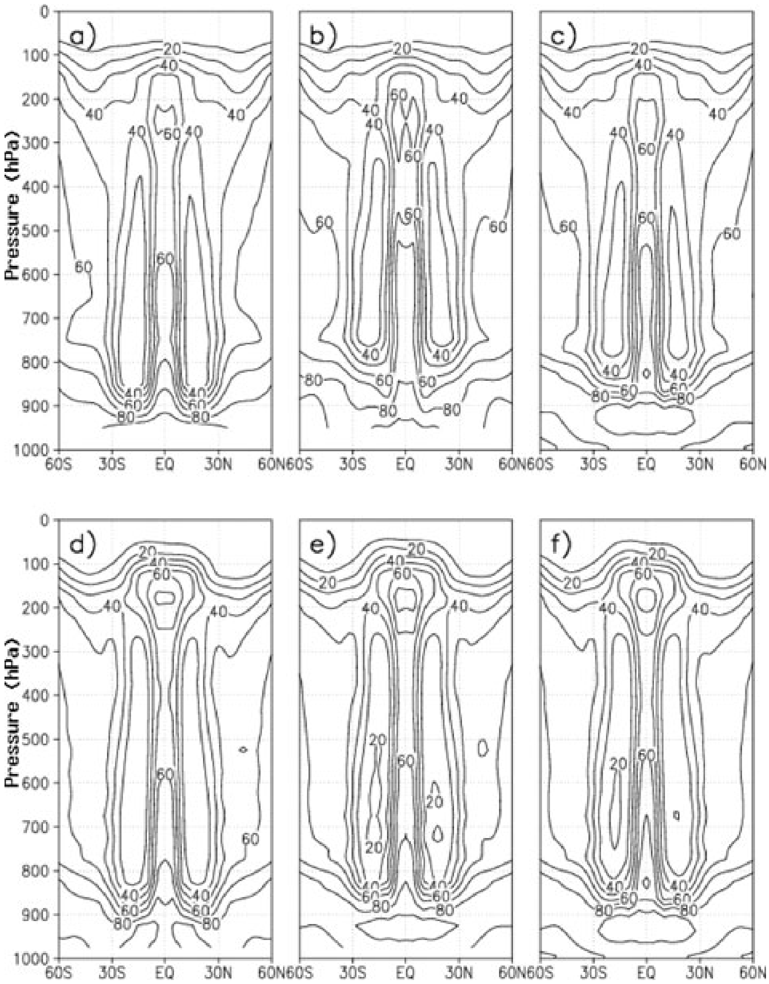

Fig. 6. (a) Zonally averaged relative humidity in percent from the Dyn10c experiment. Contour interval is 10% of relative humidity. (b) and (c) Same as (a) but for GA1021 and Dyn19, respectively. (d)–(f) Same as for (a)-(c) but for the Dyn20c, GA2029 and Dyn26 experiments, respectively.

parametrizations, where the greater impact is seen in the low-resolution experiments. The zonal wind field (not shown) does not exhibit the clear improvements in the GridAlt experiment relative to the control seen in the mass streamfunction.

The high-resolution suite of experiments in the aquaplanet framework exhibited little difference between the control (Dyn40c) and the fully resolved experiment (Dyn44). This leaves no basis by which to assess the GridAlt simulation, and it is concluded that the 25 hPa uniform vertical resolution is adequate to capture the full impact of the near-surface structure in the aquaplanet simulation.

5. Realistic suite

5.1. Experiments

To examine the impact of GridAlt at high vertical resolution (typical of decadal climate simulations) and assess its impact in realistically configured experiments, a suite of full GCM simulations with realistic land, topography and a prescribed sea surface temperature distribution was performed. The realistic suite includes two sets of experiments, each consisting of a Control and a GridAlt simulation. The first set of experiments (CtlClim and GAClim of Table 1) consists of simulations that are of 10-year duration, forced by a 50-year climatology of the weekly sea surface temperatures (SSTs) of Reynolds (1988), and the second set (CtlSST and GASST of Table 1) consists of 9-year simulations forced by the observed SSTs of Reynolds and Smith (1994). The climatological SST simulations may be regarded as 10-member ensembles of 1-year simulations, the average of which provides a statistically robust estimate of the model climatology with and without GridAlt and its additional levels for the physical forcing terms. The observed SST experiments provide the opportunity for a clear standard of success for GridAlt by direct comparison with observations and also provide an assessment of the impact of GridAlt on the simulated response to changes in SST. For all the realistic suite experiments, the land mask, topographic heights and topographic variance were interpolated from the 10 min $\times$ 10 min Navy topography data set, the surface type designations were derived from the surface classification of Defries and Townshend (1994), and information about the

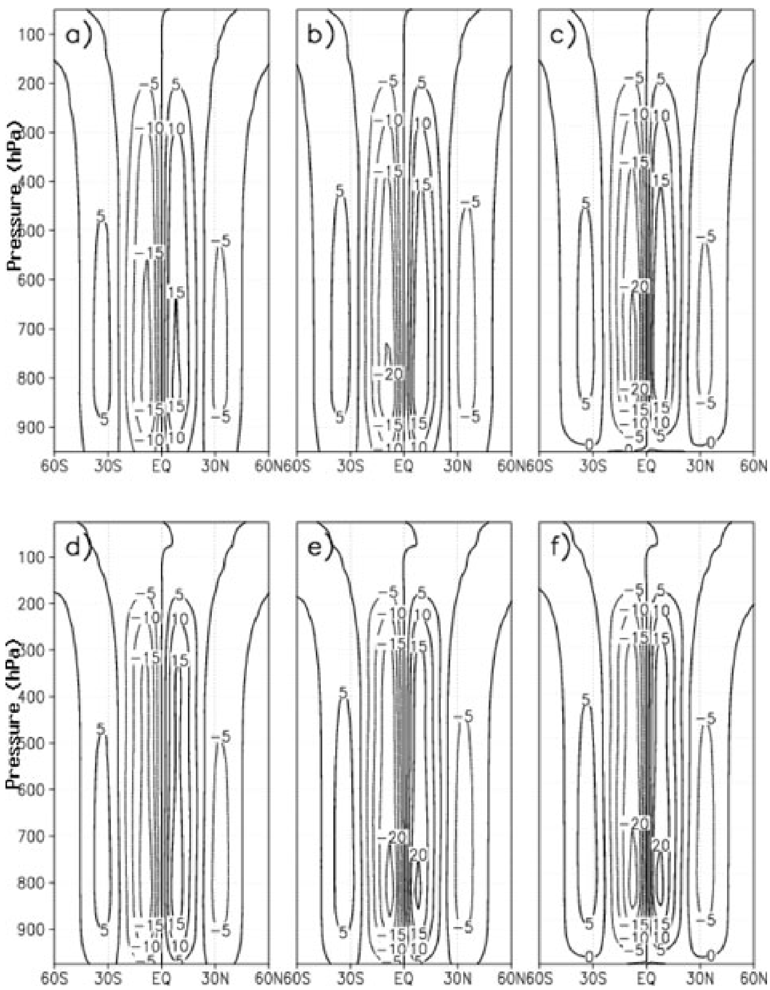

Fig. 7. (a) Zonally averaged mass streamfunction in 10^9 kg m^{-2} from the Dyn10c experiment. Contour interval is 5×10^9 kg m^{-2}. (b) and (c) Same as (a) but for GA1021 and Dyn19, respectively. (d)–(f) Same as for (a)–(c) but for the Dyn20c, GA2029 and Dyn26 experiments, respectively.

location of permanent ice was obtained from the classifications of Dorman and Sellers (1989).

The fully resolved experiment, which constituted the 'truth' for the aquaplanet suite, is not possible in this realistic framework, particularly in the MITgcm with its pressure-type p* vertical coordinate. The standard for success of GridAlt for this realistic suite, therefore, relies on comparisons with available observational estimates. NCEP (National Centers for Environmental Prediction) reanalysis (Kalnay et al., 1996) will be used here to assess the success of GridAlt in the realistic suite of experiments.

5.2. *Realistic configuration results*

As for the aquaplanet suite of experiments, the examination of the impact of GridAlt on the realistic suite of experiments begins with the physical forcing fields which are computed directly on the grid with enhanced vertical resolution. The December–January–February (DJF) and June–July–August (JJA) humidity tendency due to GCM moist processes for the Control (CtlClim) and Gridalt (GAClim) experiments is shown in Fig. 8. Again, as was apparent in the aquaplanet suite results (there the moist heating was shown, Fig. 4), the GridAlt experiment, shown in the two panels on the right hand side of Fig. 8 (panels b and d), shows an enhanced humidity tendency relative to the Control experiment. The enhancement of the humidity tendency due to moist processes in GridAlt is up to almost 1 g kg^{-1} d^{-1}, which constitutes up to a 50% increase.

Again, as for the aquaplanet experiments, the difference in behavior between the CtlClim and GAClim experiments is illustrated next with the structure of the cloud fraction, the near surface structure of which has been shown to be important for the overall climate sensitivity of the GCM simulation (Stephens, 2005). Figure 9 shows the DJF and JJA zonal mean cloud fraction from the CtlClim and GAClim experiments. As was seen in Fig. 5 for the low- and medium-resolution aquaplanet experiments, the realistic configuration GridAlt simulation results exhibit enhanced cloudiness near the boundary layer top in the

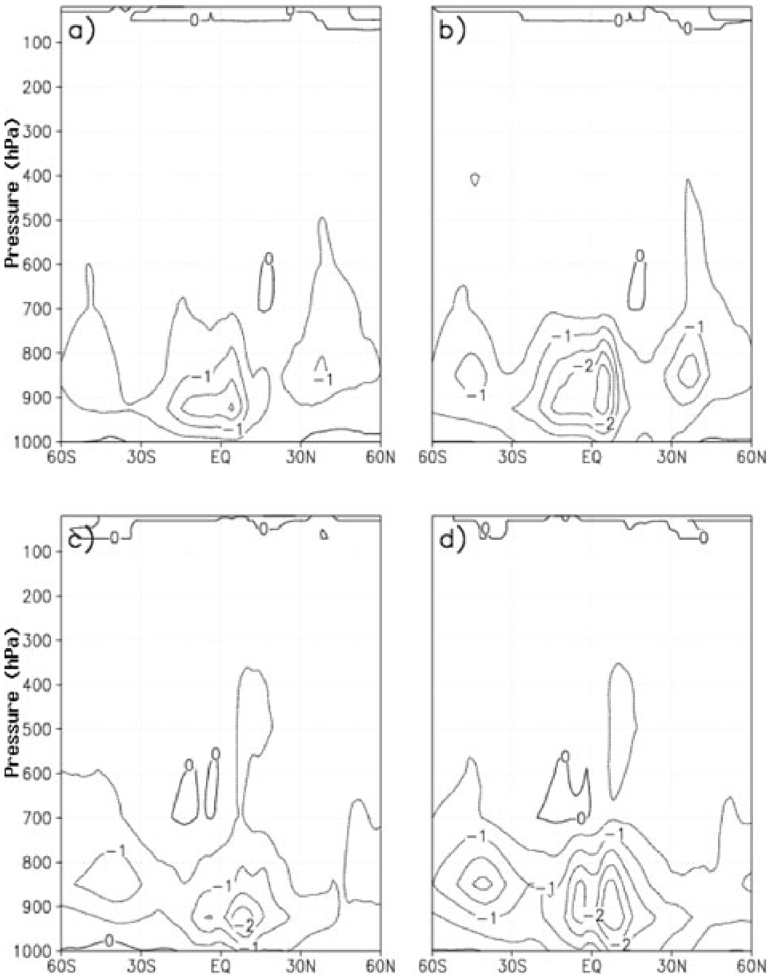

Fig. 8. (a) December–January–February averaged moist moistening in g kg^{-1} d^{-1} from the control experiment, CtlSST. Contour interval is 1 g kg^{-1} d^{-1}. (b) same as (a) but for the GridAlt experiment, GASST. (c) June–July–August averaged moist moistening in g kg^{-1} d^{-1} from CtlSST, (d) same as (c) but for GASST.

tropics relative to the Control simulation. The zonal mean differences are up to 5% of cloud fraction and represent a doubling of cloud cover in the regions of the differences.

To help understand the response of a more finely resolved atmosphere and the potential for enhanced communication between surface and atmospheric temperature variations, the thickness of the convective cloud base layer in the Control and GridAlt experiments is examined. The convective subcloud layer is diagnosed based on the vertical profile of turbulent kinetic energy and is used as the base layer or source region for shallow and deep convection. Figure 10 shows the DJF seasonal mean spatial structure of the cloud base layer thickness from the Control and GridAlt climatological SST experiments, CtlClim and GAClim. The GridAlt result (Fig. 10a) shows a closer correspondence to the underlying SST than does the Control result (Fig. 10b). The spatial pattern showing low values of cloud base thickness over cold ocean regions (darker shades of grey) and higher values of cloud base thickness over warmer oceans (lighter grey shades over the Kuroshio and Gulf Stream regions, for example) seen in Fig. 10a is not apparent in Fig. 10b. The implication of the differences in patterns is that there exists an enhanced communication of SST variations in the GridAlt simulation with its finer vertical structure in the boundary layer fields.

The final set of experiments that were analysed to assess the performance of GridAlt are the realistic climate simulations forced by observed sea surface temperatures. These experiments illustrate the impact of the use of GridAlt on the simulated response to El Niño SST variations. This is accomplished by examining the ‘Warm–Cold’, or La Niña–El Niño 300 hPa eddy height composites during DJF and comparing them with the NCEP reanalysis composite. This assessment of the response to El Niño Southern Oscillation SST variations, as well as the choice of which years make up the warm and cold composites, are after Hoerling et al. (1997). La Niña–El Niño composite eddy height fields from over the northern Pacific and continental United States are shown in Fig. 11. The GridAlt experiment result is shown in the top panel, the NCEP result in the centre panel and the Control result in the bottom panel. The negative contours over the ocean and positive contours over the continent seen in all of the panels indicate a strengthening and slight shift of

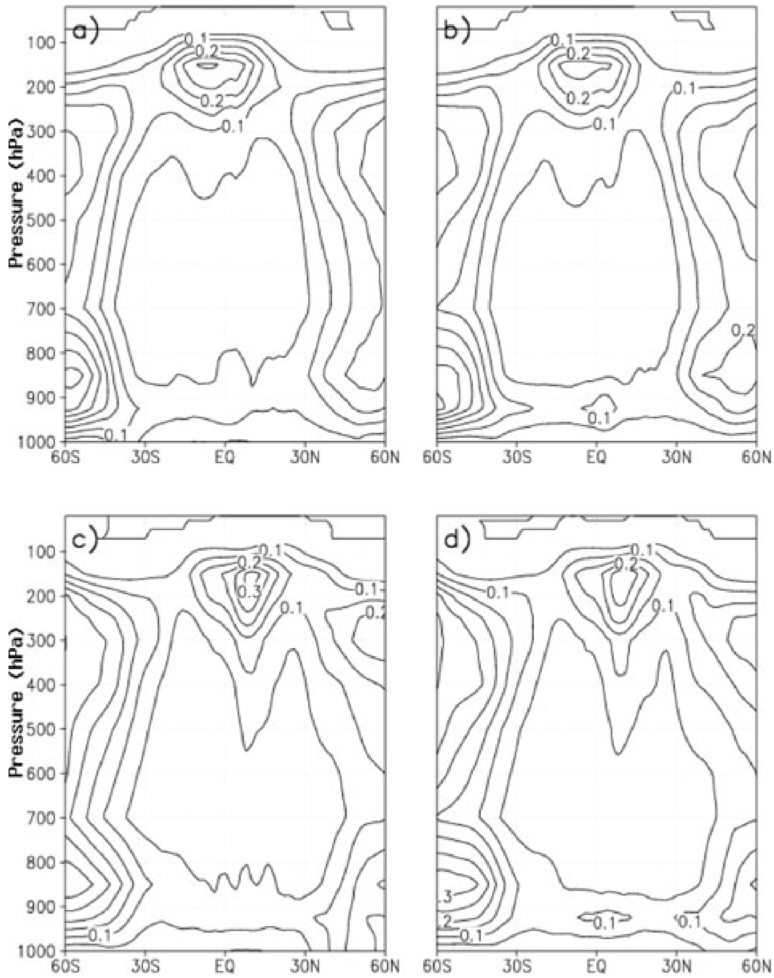

Fig. 9. (a) December–February averaged cloud fraction from the control experiment. Contour interval is 0.05. (b) same as (a) but for the GridAlt experiment. (c) June–August averaged cloud fraction from the control experiment, (d) same as (c) but for the GridAlt experiment.

the Pacific–North–America pattern of variability in the Warm–Cold composite and is mainly due to the anomalous height field during the La Niña events. Although the anomalous eddy heights are larger in magnitude in the GridAlt experiment than in the NCEP reanalysis, the pattern evident in the GridAlt experiment bears a much closer resemblance to the NCEP reanalysis than the pattern evident in the control experiment.

6. Discussion and conclusions

An 'alternate grid' technique called GridAlt has been presented, which allows physics tendencies to be computed on a separate vertical grid from the dynamics, one which enhances the vertical resolution near the surface. Results from two suites of GCM experiments, an aquaplanet suite and a realistically configured suite, were presented to evaluate the performance of GridAlt. The simplified (aquaplanet) experiments were evaluated by comparison with experiments which fully resolve the dynamics and physics on the enhanced vertical grid. For this simplified suite, the results showed that for low and medium underlying vertical resolution, the near-surface vertical structure of the 'physics tendencies' from the fully resolved simulations can be largely reproduced by using GridAlt. The impact of GridAlt on the vertical structure of the simulated mean flow was shown, where the RH and mass streamfunction of the fully resolved runs were well represented by GridAlt, but the zonal wind field was largely unaffected. The realistic suite results were evaluated against the NCEP reanalysis eddy height field. The GridAlt simulations, compared with the Control, showed enhanced vertical structure in the fields directly computed in the physical parametrizations as was evident in the aquaplanet suite and showed a better Warm–Cold ENSO composite eddy height field.

The practical benefit of the GridAlt technique for GCMs lies in the ability to capture the impact of increased vertical resolution at a potentially substantial savings in computational expense compared with running 'fully resolved' enhanced vertical resolution experiments. The largest benefit is for the low-resolution experiments in the aquaplanet suite, for which the GridAlt experiment incurs a 30% increase in wall clock time over the 10-level control, and the 'fully resolved' experiment incurs a 380% increase. For the medium resolution experiments, the GridAlt simulation

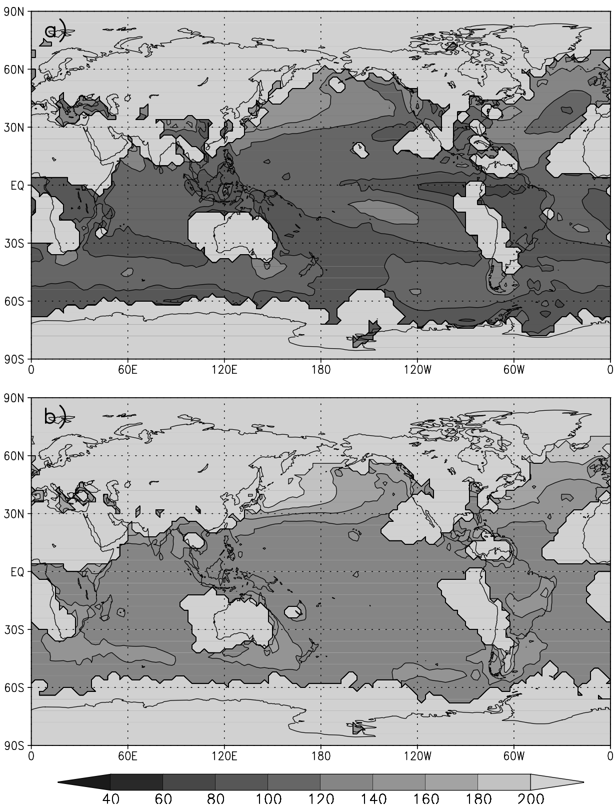

Fig. 10. (a) December–February average cloud base layer thickness in hPa from the GridAlt experiment, GASST. Contour interval is 20 hPa. (b) same as (a) but for the control experiment, CtlSST.

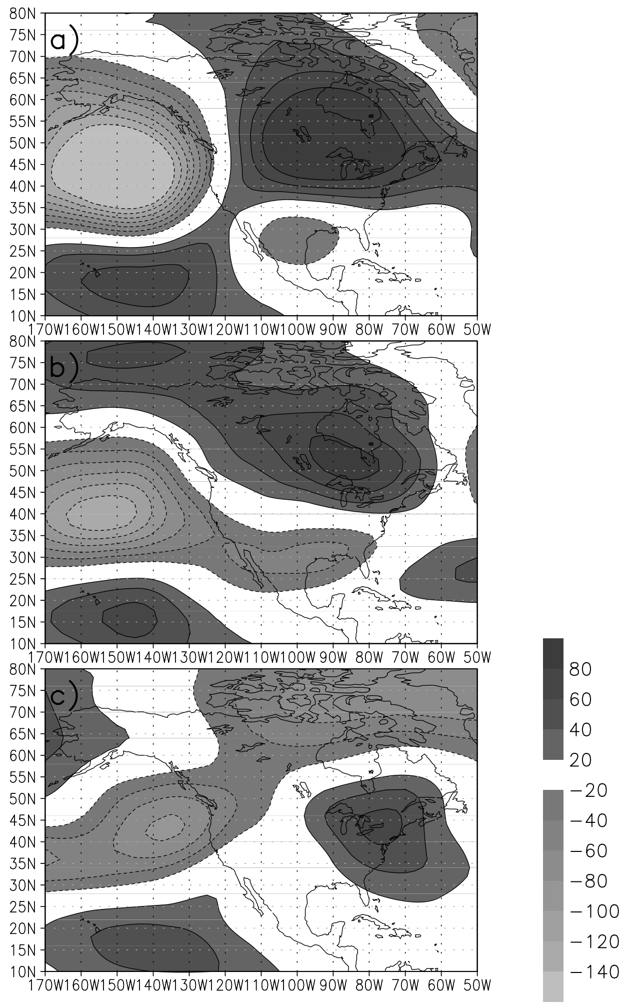

Fig. 11. Warm-cold composites of eddy height in m from: (a) GridAlt simulation, GASST; (b) NCEP reanalysis and (c) NO GridAlt simulation, CtlSST.

incurs a 7% increase in clock time relative to the control, and the ‘fully resolved’ experiment incurs a 150% increase, and for the high resolution aquaplanet experiments, the GridAlt simulation incurs an additional expense of a few percent, whereas the ‘fully resolved’ experiment incurs a 75% increase in expense. The timings are related in part to a saving in the GridAlt simulations due to the near-perfect scaling of the physics across multiple processors compared with the dynamics and, in part, to the need for a smaller time step to prevent numerical instability in the ‘fully resolved’ simulations because the near-surface levels are 3–5 mbar thick.

An underlying assumption of the GridAlt technique is that much of the benefit of increased vertical resolution near the surface can be realized by employing the higher resolution for the computation of the forcing due to the parametrizations of turbulent and convective processes in the atmosphere. The benefits for a GCM simulation have been articulated here, but there remain potentially important benefits of increased resolution that are not realized when using this technique. The dynamical response to a (vertically) localized radiative forcing, due to the presence of boundary layer clouds, for example, cannot be captured in the GridAlt simulations. One also forfeits high-resolution vertical advection with the GridAlt technique. These drawbacks notwithstanding, the GridAlt technique is an attractive solution.

Other applications of this technique within the MITgcm are in progress. Hill (2005) has applied the GridAlt technique in the MITgcm in a coarse-resolution ocean model configuration to evaluate the impact of oceanic convection evaluated on a high-resolution grid. The use of this technique for the implementation of a ‘superparametrization’ of oceanic convection also holds promise for other applications in atmospheric and oceanic GCMs.

7. Acknowledgments

The author wishes to thank Jean-Michel Campin for all the helpful consultations during the development of this work. In addition, the author thanks Chris Hill and Joe Tribbia for their insights and comments about the work and the manuscript. This work was supported under the Climate Modeling Initiative (CMI), and the computations were funded under the Alliance for Computational Earth Sciences (ACES).

References

Adcroft, A. and Campin, J.-M. 2004. Re-scaled height coordinates for accurate representation of free surface flows in ocean circulation models. *Ocean Model.* **7** 269–284.

Adcroft, A., Hill, C. and Marshall, J. 1997. Representation of topography by shaved cells in a height coordinate ocean model. *Mon. Wea. Rev.* **125**, 2293–2315.

Adcroft, A., Campin, J.-M., Hill, C. and Marshall, J. 2004. Implementation of an atmosphere-ocean general circulation model on the expanded spherical cube. *Mon. Wea. Rev.* **132**, 2845–2863.

Bushell, A. C. and Martin G. M. 1999. The impact of vertical resolution upon GCM simulations of marine stratocumulus. *Clim. Dyn.* **15**, 293–318.

Defries, R. S. and Townshend, J. R. G. 1994. NDVI-derived land cover classification at global scales. *Int. J. Remote Sens.* **15**, 3567–3586.

Dorman, J. L. and Sellers, P. J. 1989. A global climatology of albedo, roughness length and stomatal resistance for atmospheric general circulation models as represented by the Simple Biosphere model (SiB). *J. Appl. Meteorol.* **28**, 833–855.

Grabowski, W. W. 2001. Coupling cloud processes with the large-scale dynamics using the cloud-resolving convection parameterization (CRCP). *J. Atmos. Sci.* **58**, 978–997.

Hill, C. 2005. Adoption and field tests of MIT general circulation model (MITgcm) with ESMF. In: *Proceedings of the Fourth ESMF Community Meeting*, Cambridge, MA, July 20-22, 2005.

Hoerling, M., Kumar, A. and Zhong, M. 1997. El Niño, La Niña, and the nonlinearity of their teleconnections. *J. Clim.* **10**, 1769–1786.

Inness, P. M., Slingo, S. J., Woolnough, R. B., Neale, B. and Pope, V. D. 2001. Organization of tropical convection in a GCM with verying vertical resolution: implications for the simulation of the Madden-Julian oscillation. *Clim. Dyn.* **17**, 777–794.

Kalnay, E., Kanamitsu, M., Kistler, R., Collins, W., Deaven, D., Gandin, L. and co-authors. 1996. The NMC/NCAR 40-year reanalysis project. *Bull. Am. Meteorol. Soc.* **77**, 437–471.

Lock, A. 2000. The numerical representation of entrainment in parametrizations of boundary layer turbulent mixing. *Mon. Wea. Rev.* **129**, 1148–1163.

Marshall, J., Adcroft, A., Campin, J.-M. and Hill, C. 2004. Atmosphere–ocean modeling exploiting fluid isomorphisms. *Mon. Wea. Rev.* **132**, 2882–2894.

Medeiros, B. and Stevens, B. 2007. Low clouds and climate sensitivity. In: *Proceedings of the 87th AMS Annual Meeting, The Akio Arakawa Symposium*, San Antonio, TX, Jan 13–18, 2007.

Molod, A., Campin, J.-M., Hill, C. and Marshall, J. 2007. Description of the MITgcm atmospheric physics (Fizhi): algorithm and simulated climate. *MIT Center for Global Change Science Report Series, Report Number 76*, 109pp. Available at: http://web.mit.edu/cgcs/www/rpts.html.

Neale, R. B. and Hoskins, B. 2001. A standard test for AGCMs including their physical parameterizations, I: the proposal. *Atm. Sci. Lett.* **1**, doi:.

Reynolds, R. W. 1988. A real time global sea surface temperature analysis. *J. Clim.* **1**, 75–86.

Reynolds, R. W. and Smith, T. M. 1994. Improved global sea surface temperature analyses using optimum interpolation. *J. Clim.* **7**, 929–948.

Rogers, E., Black, T., Ferrier, B., Lin, Y., Parrish, D. and co-authors. 2001. Changes to the NCEP Meso Eta Analysis and Forecast System: increase in resolution, new cloud microphysics, modified precipitation assimilation, modified 3DVAR analysis. *NWS Tech. Proc. Bull,* **488**. Available at http://www.emc.ncep.noaa.gov/mmb/mmbpll/eta12tpb/

Staudenmaier, M. and Mittelstadt, H. 1997. Results of the Western Region Evaluation of the ETA-10 Model. *Western Region Tech. Attach.* **97**(18), 4pp.

Stephens, G. L. 2005. Cloud feedbacks in the climate system: a critical review. *J. Clim.* **18**, 237–273.

Vintzileos, A. and Sadourney, R. 1997. A general interface between atmospheric general circulation model and underlying ocean and land surface models: delocalized physics scheme. *Mon. Wea. Rev.* **125**, 926–941.